International Journal of Current Engineering and Technology
E-ISSN 2277 – 4106, P-ISSN 2347 – 5161

Available at http://inpressco.com/category/ijcet

Research Article

Investigating Flow Rate and Mixing Performance in Arrow Type split and Recombine Micromixers

Sanjay A. Pawar[1], Dr. Vimal Kumar Chouksey[2]

[1]Ph.D Research scholar and [2]Associate Professor, [1,2]Mechanical Engineering Department, Sardar Patel University, Balaghat, M.P, India

Received 20 Feb 2023, Accepted 07 March 2023, Available online 08 March 2023, **Vol.13, No.2 (March/April 2023)**

Abstract

The paper explores the development of micromixers for lab-on-chip applications through the stages of design, simulation, fabrication, and analysis. The primary focus is on achieving optimal mixing efficiency and film bonding stability at low Reynolds numbers, while minimizing pressure drop using cost-effective polymer microfluidic devices. Specifically, the impact of structural dimensions on mixing behavior is investigated in Split and Recombine Micro Channel using circular, square, and diamond-shaped obstacles at various Reynolds numbers ranging from 0.1 to 60. Mixing efficiency of the circular obstacle-based SAR micromixer is found to be better at a very short length without damaging the thin film bonding layer at Re 45.

Keywords: *Micromixtures, Microfluidics, Micro channel, Split and Recombine Micro Channel*

1. Introduction

"The Micromixer: An Essential Device for Microfluidic Mixing in Lab-on-a-Chip Applications. Mixing of multiple fluids in microscale channels presents a significant challenge in microfluidics due to the laminar flow behavior, making it a key area of research for applications such as chemical reactions, nano material synthesis, biological screening, biosensors, and genetic analysis (Chew, Xia, and Shu 2007; Jeong et al. 2010; Adam et al. 2014)." "Enhancing Mixing Performance in Microfluidic Channels: An Overview of Micromixers. Micromixers can be classified as either active or passive, with active micromixers requiring external energy sources such as thermal energy, magnetic fields, frequency vibration, or surface acoustic waves for mixing (Français et al. 2006; Wang et al. 2008; Oberti, Neild, and Nga 2009; Tseng et al. 2006). Passive micromixers, on the other hand, do not require external energy sources and are easier to implement. Mixing performance in passive micromixers can be improved by modifying the structural dimensions of the microchannel. Research has explored different structural dimensions to enhance mixing, including Y-shaped micromixers with rectangular and triangular obstacles (Karthikeyan, Sujatha, and Sudharsan 2017), split and recombination micromixers (Nimafar, Viktorov, and Martinelli 2012), and cylindrical obstructions within curved microchannels (Alam et al. 2014). These studies have shown mixing efficiencies ranging from 72-100% at Reynolds numbers from 0.083 to 60." "Afzal and Kim (2014) conducted a shape optimization for two-fluid mixing in a three-dimensional herringbone micromixer and obtained a mixing efficiency less than 90%. Jen et al. (2003) designed and simulated chaotic mixers with T-shaped three-dimensional structures in twisted microchannels. Most passive micromixers have different microstructures for achieving good mixing performance with high flow rate and low pressure drop. A key aspect in micromixer design is sealing the channel, for which several bonding techniques have been developed, including PDMS bonding (Cha et al. 2006), UV cured adhesive bonding (Kapilmanoharan and Lekurwale 2014), and bonding with SU8-Metal (Svasek et al. 2004). Saragih and Ko (2009) bonded a three-dimensional spring-like micromixer to the substrate using a controllable furnace."

This paper presents the fabrication and performance characteristics of three passive micromixer structures, including the Arrow Type Split and Recombine Type Micromixer with circular, diamond, and square-shaped obstacles. Typically, the pressure drop in microchannels is proportional to both the flow rate and the structural dimensions of the device. High flow rates can damage the bonding strength between the PDMS microchannel and glass substrate due to the device's structural dimensions. Therefore, it is important to determine the permissible flow rate of the micromixer device to avoid damage. To address this issue, we have introduced a low-cost thin

*Corresponding author's ORCID ID: 0000-0000-0000-0000
DOI: https://doi.org/10.14741/ijcet/v.13.2.3

film PDMS bonding technique as an alternative to existing methods such as plasma, thermal, corona discharge, and UV curing processes. Finally, we have studied the permissible flow rate and mixing efficiency of the micromixer devices mentioned above. We have also compared the mixing efficiency and pressure drop of the simulated devices for all the micromixers discussed.

2. Design of micromixer

The micromixers under investigation include the Arrow Type Split and Recombine Type Micromixer with circular, diamond, and square-shaped obstacles.

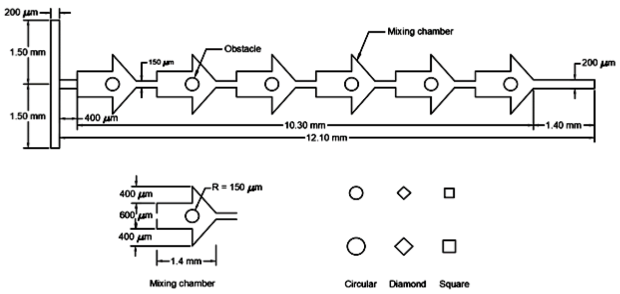

Figure 2.1: Arrow Type Split and Recombine Type Micromixer with Circular shaped Obstacle, Diamond shaped Obstacle, Square shaped Obstacle

To mix two liquids A and B, Arrow Type Split and Recombine Type Micromixer with circular, diamond, and square-shaped obstacles are employed. The micro mixer consists of a long Arrow Type channel of approximately 12.10 mm length with two inlets, each around 1500 μm in length. The micro-channel width is 200 μm, and the inlet and outlet reservoirs have a diameter of 3000 μm. Circular, diamond, and square-shaped obstacles with a radius of 150 μm, 200 μm are used, and their dimensions are illustrated in Figure 2.1.

3. Simulations of micromixers

Simulations were carried out with COMSOL Multiphysics CAD tool. The structures were drawn using the design values given in the previous section.

3.1 Micro mixture Performance Criteria

A statistical metric that indicates the uniform level of species concentration in a particular fluid is the mixing index. The mixing index of the species at any cross section in micro channel is calculated using following equation [1]:

$$M = 1 - \sqrt{\frac{1}{N}\sum_{i=1}^{N}\left(\frac{Ci-\bar{C}}{\bar{C}}\right)^2} \qquad (1)$$

Where, M is the mixing index,

N is total number of grid points

C_i is the normalized concentration at any cross section

$\bar{C}$ is the average normalized concentration of the domain.

Mixing index ranges from 0 to 1 (M = 0 for no mixing and M = 1 for 100 % mixing).

Pressure Drop

Better and quicker mixing demand flow restrictions or obstructions, which results in drop in fluid pressure. Thus, one of the most important design considerations for a micro-fluidic channel design is to minimize the pressure drop. The pressure drop in a straight rectangular channel is mainly due to friction and is determined by using the Darcy-Weisbach equation [27] which can be expressed as:

$$\Delta P = \left[\frac{f\times Re}{2}\right] \times \left[\frac{\mu\times u\times L}{(D_h)^2}\right] \qquad (2)$$

Where, ΔP is the pressure difference within the channel in Pa and L is channel length in mm.

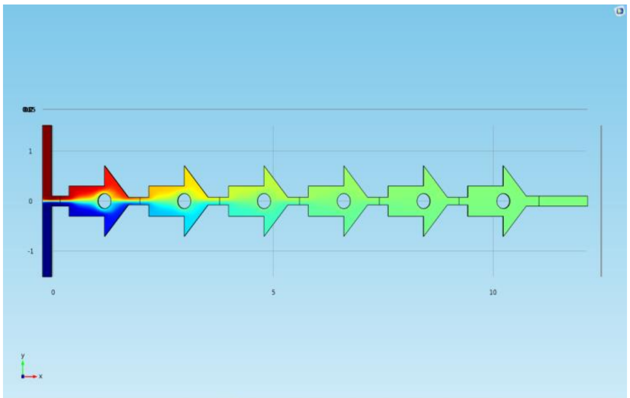

Figure 3.1: simulated result for the Reynold number 0.1 for Circular shaped obstacles

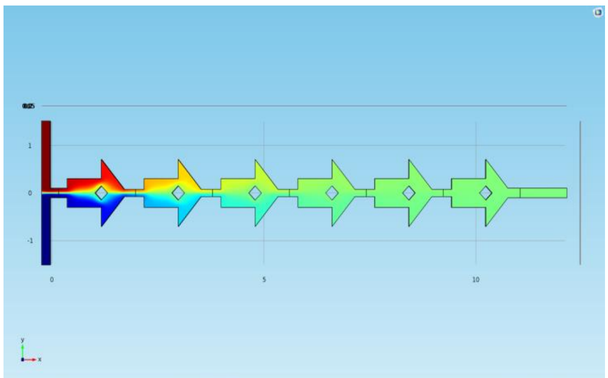

Figure3.2: simulated result for the Reynold number 0.1 for Diamond shaped obstacles

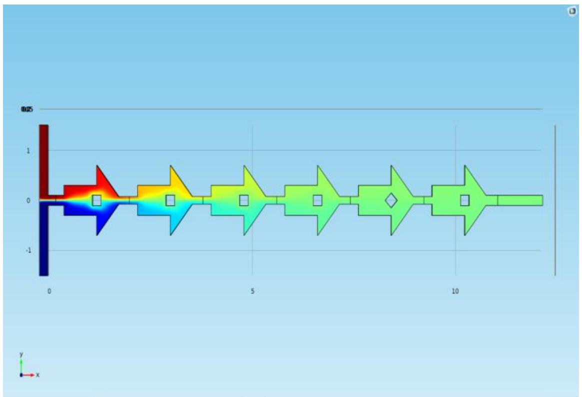

Figure 3.3: simulated result for the Reynold number 0.1 for Square shaped Obstacle

The Figure: 3.4 shows computational analysis investigates the impact of Reynolds number (Re) on the mixing index by varying Re at values of 0.1, 1, 5, 10, 15, 30, 45, and 60. The mixing index is calculated by measuring the concentration at a specific location for all considered Re values. Concentration profiles for Arrow Type SAR with circular obstacles of 150 µm and 200 µm. at eight different Re values (0.1, 1, 5, 10, 15, 30, 45, and 60) are presented.

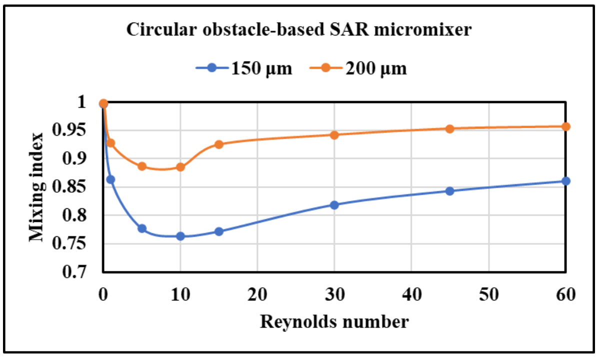

Figure 3.4: Mixing index as a function of Reynolds number for Circular Obstacle-based SAR micromixer

The Figure: 3.5 shows computational analysis investigates the impact of Reynolds number (Re) Concentration profiles for Arrow Type SAR with diamond Obstacle 150 µm and 200 µm. at eight different Re values (0.1, 1, 5, 10, 15, 30, 45, and 60) are presented.

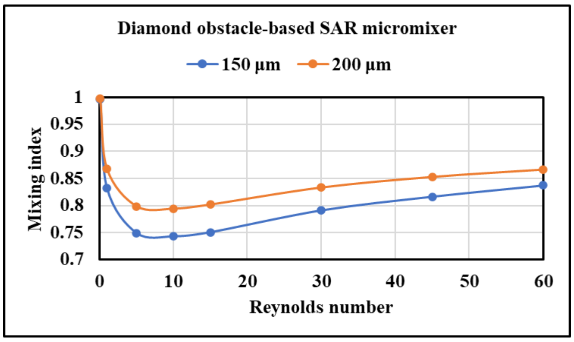

Figure. 3.5: Mixing Index as a function of Reynolds number for diamond Obstacle-based SAR micromixer

The Figure: 3.6 shows computational analysis investigates the impact of Reynolds number (Re) Concentration profiles for Arrow Type SAR with square obstacle 150 µm and 200 µm. at eight different Re values (0.1, 1, 5, 10, 15, 30, 45, and 60) are presented.

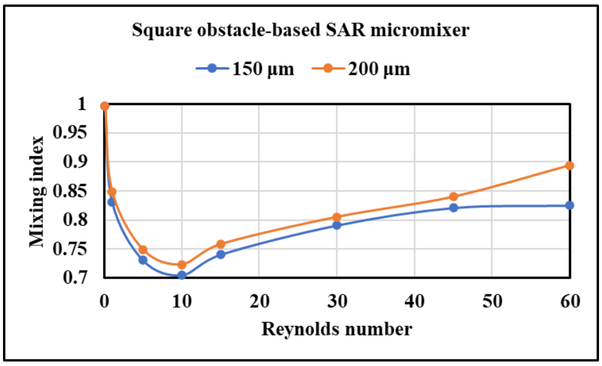

Figure 3.6: Mixing index as a function of Reynolds number for square obstacle-based SAR micromixer

The results presented in Figures 3.4, 3.5, and 3.6 demonstrate that the mixing index is highest at Re 0.1 and decreases as Re increases up to 10. Subsequently, the mixing index increases with increasing Re from 10 to 60. This trend is observed for Arrow Type SAR with circular obstacles, diamond obstacles, and square obstacles with sizes of both 150 µm and 200 µm.

At Re 0.1, higher mixing indices are observed for both Arrow Type SAR micromixers with circular obstacles of sizes 150µm and 200µm compared to Diamond shaped Obstacle and Square shaped Obstacle because diffusion is the only mixing mechanism at this lower Reynolds number. As the Reynolds number increases from 0.1 to 10, the fluid has less time for diffusion and there is no significant advection and growth of secondary flows, causing the mixing index to decrease. However, with further increase in Re from 10 to 60, the mixing index gradually increases due to the advection effect becoming more significant and the generation of secondary flows becoming more prominent. With an increase in the size of obstacles from 150µm to 200µm, advection becomes more significant, enhancing secondary flow generation and leading to better mixing performance. Thus, the mixing index for Arrow Type SAR with circular obstacles of sizes 150µm and 200µm is observed to be higher compared to Diamond shaped Obstacle and Square shaped Obstacle

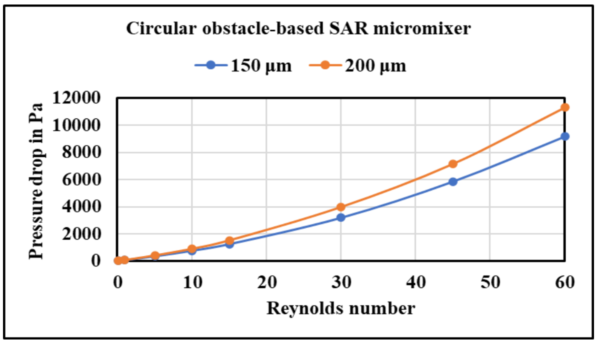

Figure 3.7: Pressure drop as a function of Reynolds number for Circular Obstacle-based SAR micromixer

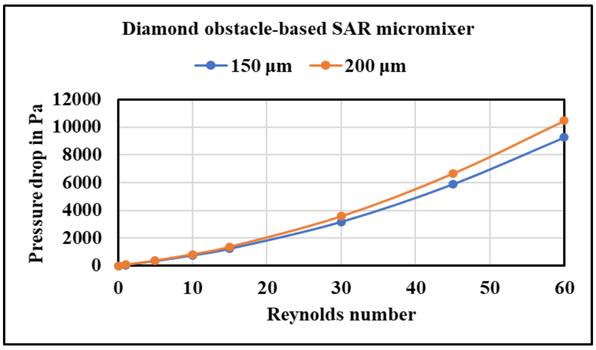

Figure 3.8: Pressure drop as a function of Reynolds number for diamond Obstacle-based SAR micromixer

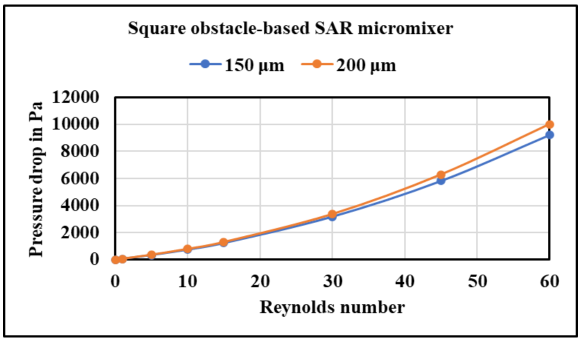

Figure 3.9: Pressure drop as a function of Reynolds number for square Obstacle-based SAR micromixer

The data presented in Figures 3.7, 3.8, and 3.9 indicate that there is a positive correlation between pressure drop and Reynolds number. The SAR design featuring circular obstacles with a size of 150 µm and square obstacles exhibit the minimum pressure drop, while the arrow type SAR design featuring circular obstacles with a size of 200 µm and diamond-shaped obstacles have the highest pressure drop. The presence of obstacles in the flow direction creates restrictions that impede the flow and result in an increase in pressure drop. As the size of the obstacles increases, the pressure drop also increases.

4. Fabrication of Arrow Type micromixers

4.1 Processes involved in fabrication of prime mould micromixer device

To create the prime mold, SU8 2075 was utilized via a UV lithography process. A silicon substrate measuring 50 mm x 50 mm was spin-coated with 3 ml of SU8 2075 negative photoresist for 10 seconds at 500 rpm, then ramped up to 2200 rpm for 30 seconds. Following this, the sample underwent pre-baking for 5 minutes at 65°C and 12 minutes at 95°C. Next, the sample was exposed to UV (365 nm) for 12 seconds and then post-baked for 5 minutes at 65°C and 10 minutes at 95°C. The sample was then developed for 20 seconds using an ultrasonic bath with SU8 developer solution, which is a fast and effective method compared to dip and immerse types of developing methods. The ultrasonication time varies based on the thickness of SU8 layers. The photoresist-develop process continued until the white precipitation disappeared and the desired pattern was achieved. The sample was then washed with IPA and deionized water before being hard-baked for 1 hour at 95°C (Karthikeyan and Sujatha, 2017)

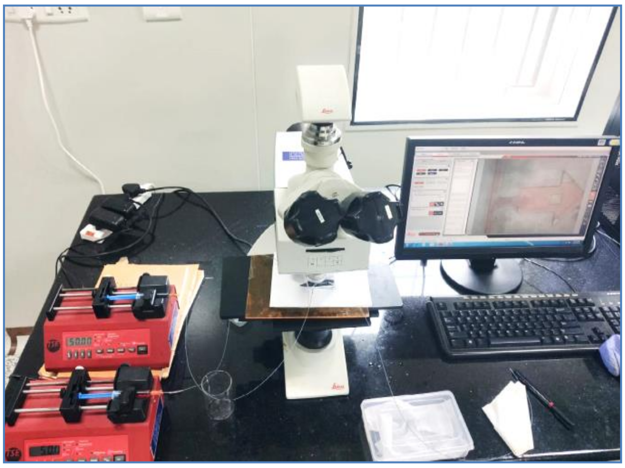

Figure 4.1: Graphical illustration of Experimental setup

Computational	Microscopic image of Experimental result	Time
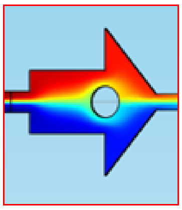	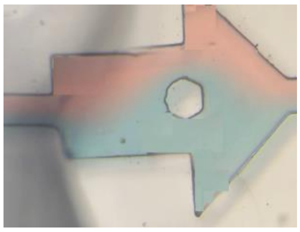	At starting
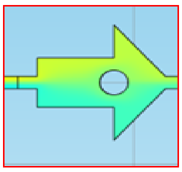	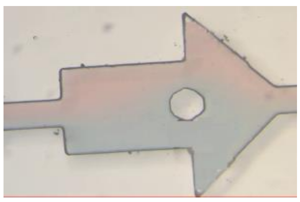	At middle
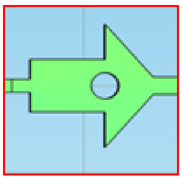	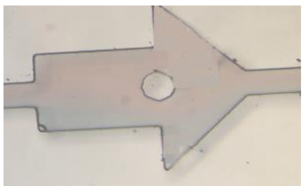	At end

Figure 4.2: simulated result and Experimental result of Circular Obstacle-based SAR micromixer

Computational result	Microscopic image of Experimental result	Time
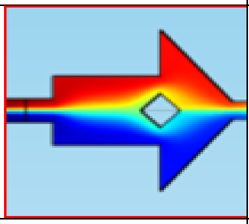	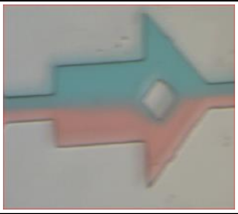	At starting
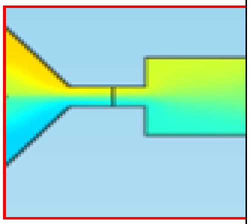	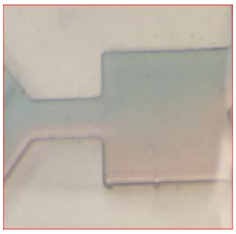	At middle
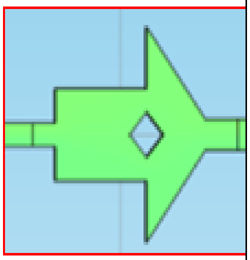	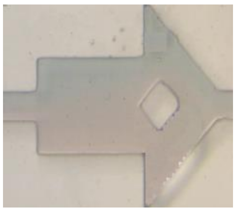	At end

Figure 4.3: simulated result and Experimental result of diamond Obstacle based SAR micromixer

Computational result	Microscopic image of Experimental result	Time
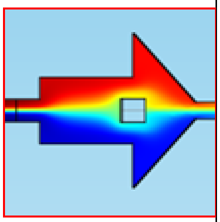	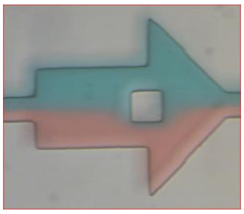	At starting
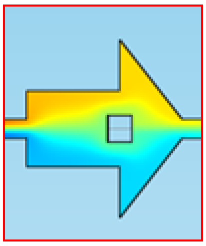	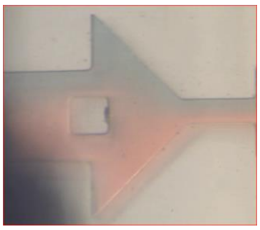	At middle
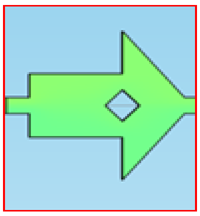	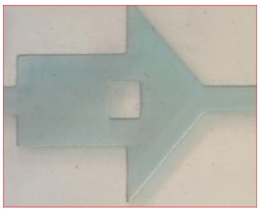	At end

Figure 4.4: simulated result and Experimental result of square Obstacle based SAR micromixer

The mixing index of the fabricated microchannels were evaluated experimentally by capturing images at different mixing lengths in the direction of flow as shown Fig. 4.2, Fig.4.3 and Fig. 4.4. The mixing index were also generated from the computational model using Eq. (1) and compared with the experimentally obtained mixing indices for circular shaped obstacles, diamond obstacles, and square obstacles with an obstacle size of 150 μm radius. It was found that circular shaped obstacles had a higher mixing index compared to diamond obstacles and square obstacles, as shown in Fig. 4.5.

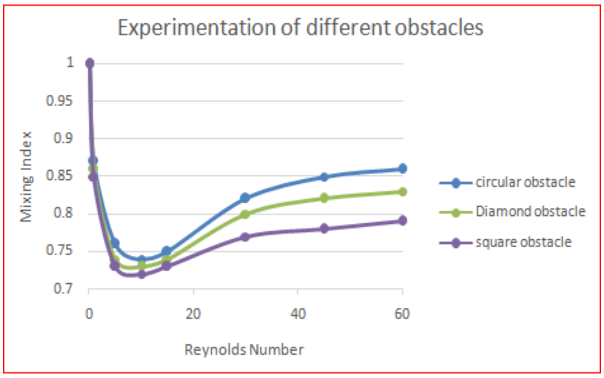

Figure 4.5: Experimental result of circular, diamond, square Obstacle based SAR micromixer

Conclusion

This study describes the design, simulation, and fabrication of passive micromixers with circular, square, and diamond-shaped obstacles. The pressure drop and mixing index are evaluated at various Reynolds numbers ranging from 0.1 to 60 and microchannel lengths. The devices are fabricated using a soft lithography technique, and bonding with the glass substrate is achieved using a thin PDMS adhesive layer. The circular obstacle-based SAR micromixer shows better mixing efficiency than the diamond and square obstacle-based SAR micromixers. The permissible Reynolds numbers of the fabricated micromixer devices are optimized, and the mixing efficiency of the circular obstacle-based SAR micromixer is found to be better at a very short length without damaging the thin film bonding layer at Re 45. Therefore, this type of micromixer is more suitable for low diffusivity fluids and low flow rate applications, such as enzyme immobilization, biosensor and diagnostic devices that require low input energy, increased stability, repeatability and longer device lifespan.

References

[1] Lee, C. Y., Wang, W. T., Liu, C. C., & Fu, L. M. (2016). Passive mixers in microfluidic systems: A review. Chemical Engineering Journal, 288, 146-160.

[2] Adam, T., Hashim, U., Dhahi, T. S., & Ud, M. N. (2014). Fabrication of Micro-Mixer for Life Sciences Applications. Ieee, 15(3), 2166-662

[3] Afzal, A., & Kim, K. Y. (2014). Three-objective optimization of a staggered herringbone micromixer. Sensors and Actuators B: Chemical, 192, 350-360

[4] Alam, A., Afzal, A., & Kim, K. Y. (2014). Mixing performance of a planar micromixer with circular obstructions in a curved microchannel. Chemical Engineering Research and Design, 92(3), 423-434

[5] Cai, G., Xue, L., Zhang, H., & Lin, J. (2017). A review on micromixers. Micromachines, 8(9), 274.

[6] Chew, Y. T., Xia, H. M., & Shu, C. (2007). Fluid micromixing technology and its applications for biological and chemical processes. In 3rd Kuala Lumpur International Conference on Biomedical Engineering 2006: Biomed 2006, 11–14 December 2006 Kuala Lumpur, Malaysia (pp. 16-20).

[7] Lim, Y. C., Kouzani, A. Z., & Duan, W. (2010). Lab-on-a-chip: a component view. Microsystem Technologies, 16, 1995-2015.

[8] Capretto, L., Cheng, W., Hill, M., & Zhang, X. (2011). Micromixing within microfluidic devices. Microfluidics: technologies and applications, 27-68..

[9] Bahrami, M., Yovanovich, M. M., & Culham, J. R. (2006). Pressure drop of fully developed, laminar flow in rough microtubes..

[10] Song, H., Wang, Y., & Pant, K. (2012). Cross-stream diffusion under pressure-driven flow in microchannels with arbitrary aspect ratios: a phase diagram study using a three-dimensional analytical model. Microfluidics and nanofluidics, 12, 265-277..

[11] Ansari, M. A., Kim, K. Y., & Kim, S. M. (2010). Numerical study of the effect on mixing of the position of fluid stream interfaces in a rectangular microchannel. Microsystem technologies, 16, 1757-1763.Gobby, D., Angeli, P. and Gavriilidis, A., 2001. Mixing characteristics of T-type microfluidic mixers. Journal of Micromechanics and microengineering, 11(2), p.126.

[12] Bothe, D., Stemich, C., & Warnecke, H. J. (2006). Fluid mixing in a T-shaped micro-mixer. Chemical engineering science, 61(9), 2950-2958.Virk, M.S. and Holdø, A.E., 2016. Numerical analysis of fluid mixing in T-Type micro mixer. The International Journal of Multiphysics, 2(1).

[13] Cortes-Quiroz, C. A., Azarbadegan, A., & Zangeneh, M. (2014). Evaluation of flow characteristics that give higher mixing performance in the 3-D T-mixer versus the typical T-mixer. Sensors and Actuators B: Chemical, 202, 1209-1219.

[14] Lü, Y., Zhu, S., Wang, K., & Luo, G. (2016). Simulation of the mixing process in a straight tube with sudden changed cross-section. Chinese journal of chemical engineering, 24(6), 711-718.

[15] Naher, S., Orpen, D., Brabazon, D., Poulsen, C. R., & Morshed, M. M. (2011). Effect of micro-channel geometry on fluid flow and mixing. Simulation Modelling Practice and Theory, 19(4), 1088-1095.

[16] Ansari, M. A. (2009). Parametric study on mixing of two fluids in a three-dimensional serpentine microchannel. Chemical Engineering Journal, 146(3), 439-448.

[17] Liu, J., Li, S., & Mitra, D. (2015). Multiphysical phenomenon of air bubble growth in polydimethylsiloxane channel corners under microfluidic negative pressure-driven flow. International Journal of Heat and Mass Transfer, 91, 611-618..

[18] Liu, R. H., Stremler, M. A., Sharp, K. V., Olsen, M. G., Santiago, J. G., Adrian, R. J., ... & Beebe, D. J. (2000). Passive mixing in a three-dimensional serpentine microchannel. Journal of microelectromechanical systems, 9(2), 190-197.

[19] Kuo, J. N., & Jiang, L. R. (2014). Design optimization of micromixer with square-wave microchannel on compact disk microfluidic platform. Microsystem technologies, 20, 91-99.

[20] Kuo, J. N., & Chen, X. F. (2016). Decanting and mixing of supernatant human blood plasma on centrifugal microfluidic platform. Microsystem Technologies, 22, 861-869.

[21] Kuo, J.N. and Li, Y.S., 2017. Centrifuge-based micromixer with three-dimensional square-wave microchannel for blood plasma mixing. Microsystem Technologies, 23(7), pp.2343-2354.

[22] Xia, G., Li, J., Tian, X., & Zhou, M. (2012). Analysis of flow and mixing characteristics of planar asymmetric split-and-recombine (P-SAR) micromixers with fan-shaped cavities. Industrial & engineering chemistry research, 51(22), 7816-7827.

[23] Li, J., Xia, G., & Li, Y. (2013). Numerical and experimental analyses of planar asymmetric split-and-recombine micromixer with dislocation sub-channels. Journal of Chemical Technology & Biotechnology, 88(9), 1757-1765.

[24] Tran-Minh, N., Dong, T., & Karlsen, F. (2014). An efficient passive planar micromixer with ellipse-like micropillars for continuous mixing of human blood. Computer methods and programs in biomedicine, 117(1), 20-29..

[25] Ta, B. Q., Le Thanh, H., Dong, T., Thoi, T. N., & Karlsen, F. (2015). Geometric effects on mixing performance in a novel passive micromixer with trapezoidal-zigzag channels. Journal of micromechanics and microengineering, 25(9), 094004..

[26] Cortes-Quiroz, C. A., Zangeneh, M., & Goto, A. (2009). On multi-objective optimization of geometry of staggered herringbone micromixer. Microfluidics and nanofluidics, 7, 29-43.

[27] Juraeva, M., & Kang, D. J. (2020). Mixing performance of a cross-channel split-and-recombine micro-mixer combined with mixing cell. Micromachines, 11(7), 685.

[28] Shinde, A. B., Patil, A. V., & Patil, V. B. (2021). Enhance the mixing performance of water and ethanol at micro level using geometrical modifications. Materials Today: Proceedings, 46, 460-470.

[29] Hossain, S., Fuwad, A., Kim, K. Y., Jeon, T. J., & Kim, S. M. (2020). Investigation of mixing performance of two-dimensional micromixer using Tesla structures with different shapes of obstacles. Industrial & Engineering Chemistry Research, 59(9), 3636-3643..

[30] Gidde, R. R. (2021). On the computational analysis of short mixing length planar split and recombine micromixers for microfluidic applications. International journal of environmental analytical chemistry, 101(1), 79-94.

[31] Raza, W., Hossain, S., & Kim, K. Y. (2020). A review of passive micromixers with a comparative analysis. Micromachines, 11(5), 455..

[32] Fuwad, A., Hossain, S., Ryu, H., Ansari, M. A., Khan, M. S. I., Kim, K. Y. & Kim, S. M. (2020). Numerical and experimental study on mixing in chaotic micromixers with crossing structures. Chemical Engineering & Technology, 43(9), 1866-1875.